We are IntechOpen, the world's leading publisher of Open Access books
Built by scientists, for scientists

4,400
Open access books available

118,000
International authors and editors

130M
Downloads

154
Countries delivered to

Our authors are among the

TOP 1%
most cited scientists

12.2%
Contributors from top 500 universities

CLARIVATE ANALYTICS
BOOK CITATION INDEX
INDEXED

WEB OF SCIENCE™

Selection of our books indexed in the Book Citation Index
in Web of Science™ Core Collection (BKCI)

Interested in publishing with us?
Contact book.department@intechopen.com

Numbers displayed above are based on latest data collected.
For more information visit www.intechopen.com

Heat Generation and Removal in Fiber Lasers

Maryam Eilchi and Parviz Parvin

Additional information is available at the end of the chapter

Abstract

The present chapter looks at heat generation and heat removal in fiber lasers, particularly if high–power or high–energy operation is required. In the context of the review, for the purpose of calculation of heat dissipation for different parts of the active gain media and providing effective cooling procedures, thermal loading as well as longitudinal and transverse temperature profiles of dual–clad fibers are comprehensively investigated both inside and outside of the doped fiber core. Considering numerical analysis, the heat deposited in the fiber due to pump and laser power is determined via the steady–state equations and also transient conductive, convective, as well as radiative heat transfer equations. Besides this, important features regarding how to mitigate thermal effects are stated. On the other hand, we will show that chilling mechanisms are very efficient methods for dissipating heat which is extensively adopted in high–power regimes. Finally, the concept of a cryogenic laser is discussed after propounding a novel cooling system, namely the dry–ice chiller.

Keywords: Thermal effects, heat dissipation, temperature treatment, conductive, convective and radiative heat transfer equations, cryogenic lasers, cooling

1. Introduction

Due to eminent efficiency, good compactness and reliability, outstanding spatial beam quality, efficient heat dissipation, and freedom from thermal lensing, fiber lasers are now competing with their bulk solid–state counterparts for interesting scientific and industrial applications [1–3] such as material processing, defense, remote sensing, free–space communication, etc. With the availability of high–power and high–brightness laser diodes accompanied with cladding pumped architecture, a rise in output power from ytterbium (Yb)–doped, double–clad fiber laser sources has been dramatic recently, maturing to the point of hundreds of Watts [4–6], even in the case of continuous–wave (CW) regimes, 10/50 kW for single–transverse–mode/multi–mode operations [7], and beyond.

Thanks to the long and thin fiber geometries, stress fracture and beam distortion, which are major problems for bulk solid–state lasers, can both be alleviated in fiber lasers. However, heat management and nonlinear effects, i.e., stimulated Brillouin and Raman scatterings (SBS and SRS), are still the most critical issues for scaling higher output powers [8]. By utilizing large mode area (LMA) fibers and broadening the spectral bandwidth of the seeding signal, the latter can be effectively suppressed.

Fiber lasers inherently exhibit exceptional capacity for heat dissipation, facilitated by very long and thin fiber cylinders with a large surface area to active volume ratio. In practice, the physical design to eliminate nonlinearities deteriorates thermal management in high–power regimes [9–11] and hence increases the threshold to thermal lensing features. One should keep in mind that double–clad optical fibers are surrounded by a low index polymer coating with limited tolerance to heat (~150–200 °C) [12], while the core temperature is always located below the melting point of quartz (1982 K) [13].

The majority of the heat converted from the optical power takes place in the fiber core, where most of the pump power is absorbed. The maximum temperature is hence expected to appear at the fiber axis. The fraction of power turned into heat due to quantum defect is defined as the ratio of pump–to–signal wavelengths, however, the actual heat fraction depends on the detailed kinetics of the system being used [14].

It is worth nothing that, whilst the fiber laser is immune to thermal effects to a large extent at low powers, there are significant characteristics and major restrictions in a kilowatt power domain [15–16] which influence laser performance and cannot be ignored. In one embodiment, pump–induced heating can cause a number of serious problems, comprising;

- formation of thermal cracks due to internal thermal stress and expansion;
- shortening of fiber lifetime owing to damage of fiber coatings, even melting of the glass;
- degradation of laser beam quality due to thermal lensing;
- deterioration of optical coupling efficiency affected by the undesirable temperature–induced motion of mechanical parts;
- enhancement of mode instability [17–18] and mode distortion [19];
- reduction of laser quantum efficiency and gain coefficient; and finally
- intensification of threshold power.

Another approach implies that fiber fractures may be distinguished at high average power under pulsed operation.

From another point of view, the question of how to optimize fiber and pump conditions in order to facilitate heat dissipation is critical at any kilowatt level. Once an appropriate distribution of operating temperatures is considered for the whole fiber, other issues like thermo–optic effects, fiber lifetime, and mechanical stability are easily diminished [20]. Thus, it is important to investigate an accurate model for estimating temperature along the fiber, and then to supply appropriate cooling techniques.

There are some solutions to drastically lower the operating temperature for double–clad fiber lasers including active or passive efficient cooling [21]. Increasing of gain, beam quality, thermal conductivity, as well as efficiency, together with reducing the thermal expansion and thermo–optic coefficients, temperature gradients, thermal lensing, self–pulsing [22], thermally induced broadening, saturation, and threshold powers are the main approaches used in such chilling systems but at the cost of raising spectral linewidth [23]. Synthesizing those factors in cryogenically cooled systems allows for strong improvements in master–oscillator and power–amplifier performance.

This chapter emphasizes the understanding of heat generation and removal concerned with fiber laser amplifiers. A comprehensive review is provided to predict thermal treatment along the active media in Section 2. Particular focus is placed on theoretically analyzing the pump–induced temperature change, applicable for a couple of CW and pulsed modes for optical fiber lasers and amplifiers. Additionally, three–dimensional (3D) simulation is implemented both for axial and transverse thermal distributions by means of conductive, convective, as well as radiative heat transfer relations. In the final section, significant chilling procedures are introduced, including air and liquid cooling, thermoelectric heat sinks, dry–ice chillers, and the concept of cryogenic lasers, etc.

2. Theory

In order to improve laser performance and decrease thermal destructive effects, temperature evolution must be determined within the fiber laser which relies on the pump beam intensity profile, thermal properties (glass fiber and cladding materials), geometry, and cooling medium [24].

In all optical doped fibers, thermal effects are associated with absorbing a finite amount of optical power by the active gain media. If the electronic relaxation of the dopant involves non–radiative processes, heat is generated. For high–power regimes, thermal effects can limit the maximum pump power that can be delivered to the fiber and therefore the maximum output power [25] which can be extracted. In turn, this can mitigate the maximum seed signal injected in booster amplifiers and fiber attenuators.

Herein, explicit expressions for the thermal behavior made by the pump or lasing power, as well as heat deposited both inside and outside of the fiber core, are derived by analytically solving the heat diffusion equation [26–28]. In general terms, we consider only the case where the core and cladding regions are concentric. This assumption can also be readily modified in a more advanced treatment of the scaling effects and is not expected to influence the substance of our conclusions.

By presuming circular cross–sectional areas seen in Figure 1, there are three distinct regions for double–clad fibers that need to be addressed: (I) the core, (II) the inner cladding, and (III) the outer cladding zones. The quantities a, b, and c indicate the core, inner, and outer cladding radii, respectively.
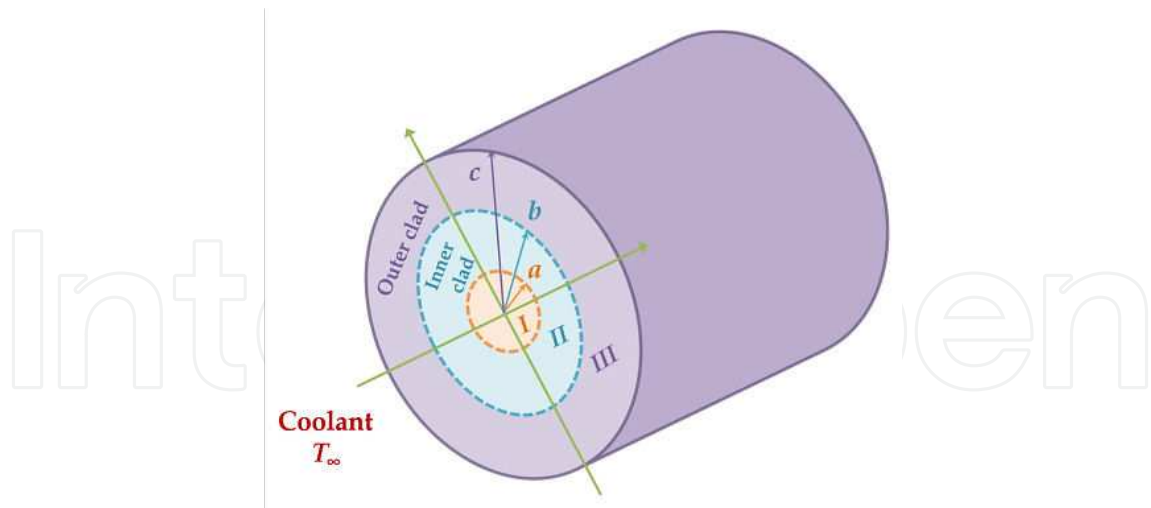
Figure 1. The geometry of various layers of a typical dual–clad fiber.

Commonly, the general form of the heat conduction equation in an isotropic medium in order to determine the time–dependent 3D temdperature distribution can be written as:

$$\rho c_v \frac{\partial T(r,\varphi,z,t)}{\partial t} - \kappa \nabla^2 T(r,\varphi,z,t) = Q(r,\varphi,z,t) \tag{1}$$

Here, T illustrates the temperature, the radial/axial coordinate is r/z, φ the azimuthal angle, and t denotes the time. Moreover, κ shows the thermal conductivity of the fiber and the dissipated heat density per unit volume that is created in the fiber core is displayed as $Q(r,\varphi,z,t)$. In addition, ρ and c_v demonstrate the mass density of the material and the specific heat capacity at a constant volume, respectively.

2.1. CW Mode

2.1.1. Transverse thermal analysis

In what follows, we focus on the case where the deposition of heat density into the fiber is uniform, $Q(r,\varphi,z,t)=Q_0$ [29–30] which is a good approximation in long, weakly doped fibers. Note that, any azimuthal variations can be ignored for the symmetrical structure of the fiber in cylindrical coordinates. On the other hand, no z variation is taken into account ($\partial^2/\partial z^2=0$), where z is the propagation direction along the fiber.

To model thermal effects, we refer to the cladding with identifying separated layers. In the first approach, let us suppose that the core and two cladding regions are composed of similar glass, with analogous thermal and mechanical properties [26] as well as comparable temper-ature–independent parameters comprising Poisson's ratio, Young's modulus, thermal expansion, and refractive index variation. Moreover, the dominant heat profile is deposited only in the uniform core.

Regarding Figure 1, under the steady–state operation ($\partial / \partial t = 0$), the heat equation for an isotropic medium Eq. (1) can be rewritten as follows:

$$\nabla^2 T(r) = \frac{-Q_0}{\kappa} \tag{2}$$

Therefore, applying a simplifier hypothesis, the above equation can be expounded for three distinct areas:

$$\frac{1}{r}\frac{\partial}{\partial r}\left[r\frac{\partial T_1(r)}{\partial r}\right] = \frac{-Q_0}{\kappa_1} \qquad 0 \leq r \leq a \tag{3}$$

$$\frac{1}{r}\frac{\partial}{\partial r}\left[r\frac{\partial T_2(r)}{\partial r}\right] = 0 \qquad a \leq r \leq b \tag{4}$$

$$\frac{1}{r}\frac{\partial}{\partial r}\left[r\frac{\partial T_3(r)}{\partial r}\right] = 0 \qquad b \leq r \leq c \tag{5}$$

The temperatures and their derivatives must be continuous across the borders [31]. Therefore, the multipoint boundary conditions of the thermal conductive equations are given by:

$$T_1(r = a) = T_2(r = a) \text{ and } T_2(r = b) = T_3(r = b) \tag{6}$$

$$\kappa_1 \left.\frac{\partial T_1(r)}{\partial r}\right|_{r=a} = \kappa_2 \left.\frac{\partial T_2(r)}{\partial r}\right|_{r=a} \tag{7}$$

$$\kappa_2 \left.\frac{\partial T_2(r)}{\partial r}\right|_{r=b} = \kappa_3 \left.\frac{\partial T_3(r)}{\partial r}\right|_{r=b} \tag{8}$$

In addition, the temperature in the center of the core ($r = 0$) must satisfy:

$$\left.\frac{\partial T_1(r)}{\partial r}\right|_{r=0} = 0 \tag{9}$$

Yet, another boundary condition is that for ($r = c$), where Newton's law of cooling is governed, T_3 actualizes the following formula [26]:

$$\kappa_3 \left. \frac{\partial T_3}{\partial r} \right|_{r=c} = h \left[T_c - T_3 (r = c) \right] \tag{10}$$

where h is the total of the convective and radiative heat transfer coefficients and T_c ascertains the coolant temperature. Straightforward solution of Eqs (3)–(5), subject to the aforementioned boundary conditions, results in the following expressions for the temperatures in regions I, II, and III [13];

$$T_1(r) = T_0 - \frac{Q_0 r^2}{4\kappa_1} \qquad 0 \le r \le a \tag{11}$$

$$T_2(r) = T_0 - \frac{Q_0 a^2}{4\kappa_1} - \frac{Q_0 a^2}{2\kappa_2} \ln\left(\frac{r}{a}\right) \qquad a \le r \le b \tag{12}$$

$$T_3(r) = T_0 - \frac{Q_0 a^2}{4\kappa_1} - \frac{Q_0 a^2}{2\kappa_2} \ln\left(\frac{b}{a}\right) - \frac{Q_0 a^2}{2\kappa_3} \ln\left(\frac{r}{b}\right) \qquad b \le r \le c \tag{13}$$

Equation 11 shows that in the pumped core region, the temperature varies quadratically with r, while Eqs (12) and (13) reveal that the temperature logarithmically falls off. Furthermore, T_0 (the temperature of core's center), which is related to the coolant temperature, can be described by use of [13]:

$$T_0 = T_c + \frac{Q_0 a^2}{2hc} + \frac{Q_0 a^2}{4\kappa_1} + \frac{Q_0 a^2}{2\kappa_2} \ln\left(\frac{b}{a}\right) + \frac{Q_0 a^2}{2\kappa_3} \ln\left(\frac{c}{b}\right) \tag{14}$$

Besides, the average temperature T_{av} [26] can be calculated thus:

$$T_{av} = \frac{\int_0^a T_1(r)\,dr + \int_a^b T_2(r)\,dr + \int_b^c T_3(r)\,dr}{\int_0^c dr} \tag{15}$$

2.1.2. 3D thermal analysis

2.1.2.1. Analytical approach

The obtained results in the previous section can be easily extended to the non–uniform heat deposition or pump light absorption [32–33]. Therefore, Eq. (3) modifies to the following form [34–35];

$$\frac{1}{r}\frac{\partial}{\partial r}\left[r\frac{\partial T_1(r,z)}{\partial r}\right] = \frac{-Q(r,z)}{\kappa_1} \qquad 0 \le r \le a \tag{16}$$

The absorbed pump power within the fiber length is expressed as follows:

$$\Delta P_{abs} = P_p(z) - P_p(z+dz) = \frac{dP_p(z)}{dz}.\Delta z \tag{17}$$

$$\Delta Q(r,z) = (1-\eta)\Delta P_{abs} \tag{18}$$

Therefore, utilizing the definition of forward and backward pump powers [36–38], we can conclude that:

$$Q(r,z) \cong Q(z) = \frac{\alpha(z)P_p(z)}{\pi a^2}(1-\eta) \tag{19}$$

where

$$\alpha(z) = \alpha_a(z) + \alpha_s \tag{20}$$

Here, $Q(z)$ represents the heat power density along the axial direction of the fiber, η is the quantum efficiency, $\alpha_a(z)$ denotes the absorption coefficient and α_s indicates the signal scattering loss. Hence, the temperatures in the core and claddings can be derived by employing steady–state thermal conductive equations subject to boundary conditions, as below [39]:

$$T_1(r,z) = T_0 - \frac{Q(z)r^2}{4\kappa_1} \qquad 0 \le r \le a \tag{21}$$

$$T_2(r,z) = T_0 - \frac{Q(z)a^2}{4\kappa_1} - \frac{Q(z)a^2}{2\kappa_2}\ln\left(\frac{r}{a}\right) \qquad a \le r \le b \tag{22}$$

$$T_3(r,z) = T_0 - \frac{Q(z)a^2}{4\kappa_1} - \frac{Q(z)a^2}{2\kappa_2}\ln\left(\frac{b}{a}\right) - \frac{Q(z)a^2}{2\kappa_3}\ln\left(\frac{r}{b}\right) \qquad b \leq r \leq c \qquad (23)$$

In general terms, the temperature profiles are significantly affected by pump evolution along the fiber length. For example, the temperature conducts along the radial and axial directions of the fiber in forward and bidirectional pumping modes shown in Figure 2(a) and (b), respectively. It can be seen that the temperature distribution for the forward pump mode is uneven along the fiber. At the fiber axis ($r = 0$), the maximum (minimum) temperature of 357.8 °C (33.0 °C) is attained at the fiber input (output) side. Therefore, some active cooling procedures have to be taken at the input side of the fiber. As would be expected, the radial distribution of the temperature profile can be ignored while significant heat is traveling through the axial direction of the fiber.
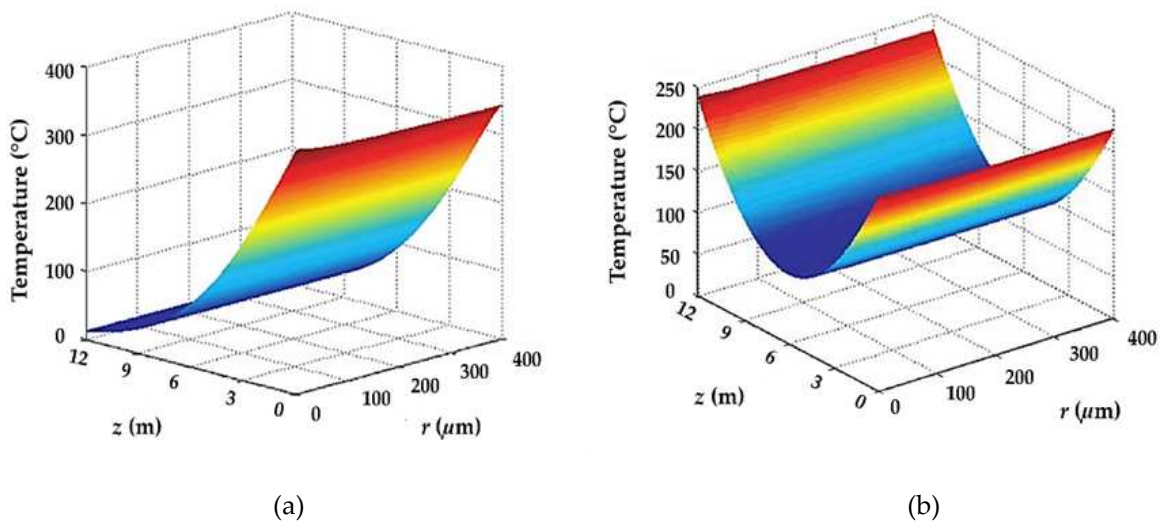

(a)   (b)

Figure 2. Evolution of temperature along both radial and axial directions of the fiber for (a) forward pump mode and, (b) bidirectional pumping configuration [35].

Analogously, according to Figure 2(b), at the fiber axis ($r = 0$), a maximum (minimum) temperature of 237.4 °C (84.2 °C) is reached at the fiber input and output sides (middle of the fiber). The maximum temperature difference in the radial direction is 7.6 °C, which is obtained at the output side.

Comparing the results of the forward pump mode with that of the bidirectional pumping configuration, one can be said that the temperature evolutions in axial and radial directions of the fiber for the two–end pump mode are more even, and the maximum temperature in the fiber is decreased by 120.4 °C. Therefore, the bidirectional pumped array is preferred here.

2.1.2.2. Numerical approach

The scope of this section relates to the case where $\partial^2/\partial z^2 \neq 0$. Here, the injected pump light is absorbed by doped ions in the fiber core. Hence, there is a heat source in the core that does not

exist in the claddings. In this case, according to the non–uniformity (exponential evolution) of the pump power in the axial direction, the Q value is not constant. On the other side, since the fiber length is much larger than the cross section, the capability of heat dissipation from the fiber end facets is much lower than from the fiber sides.

The heat dissipation as well as both transverse and longitudinal temperature distributions in a typical rare–earth doped dual–clad fiber is expressed by the following time–independent thermal conduction equation in symmetric cylindrical coordinate (r, z) [9, 15, 20, 27]:

$$\frac{1}{r}\frac{\partial}{\partial r}\left[r\frac{\partial T_1(r,z)}{\partial r}\right]+\frac{\partial^2 T_1(r,z)}{\partial z^2}=\frac{-q(r,z)}{\kappa_1} \qquad 0\leq r\leq a \tag{24}$$

$$\frac{1}{r}\frac{\partial}{\partial r}\left[r\frac{\partial T_2(r,z)}{\partial r}\right]+\frac{\partial^2 T_2(r,z)}{\partial z^2}=0 \qquad a\leq r\leq b \tag{25}$$

$$\frac{1}{r}\frac{\partial}{\partial r}\left[r\frac{\partial T_3(r,z)}{\partial r}\right]+\frac{\partial^2 T_3(r,z)}{\partial z^2}=0 \qquad b\leq r\leq c \tag{26}$$

The boundary condition at the surface between the fiber cladding and the ambient environment is given by Newton's and Stefan–Boltzmann's laws, as below [35]:

$$\kappa_3\left.\frac{\partial T_3}{\partial r}\right|_{r=c}=h(z)\left[T_c-T_3(r=c)\right] \tag{27}$$

Here, h is a function of z too [10] that can be determined using the following relations:

$$h(z)=0.5\times N_u(z).\kappa_c.c^{-1} \tag{28}$$

$$N_u(z).exp\left[\frac{-2}{N_u(z)}\right]=0.16\times\left[G_r(z).P_r\right]^{1/3} \tag{29}$$

$$G_r(z)=8g.d_c^2.c^3.\mu_c^{-2}.T_c^{-1}\left[T(r=c,z)-T_c\right] \tag{30}$$

where T indicates the temperature in the fiber, and the heat sink temperature is represented by T_c. Also, $q(r, z)$ exhibits the heat dissipated in a unit volume, chiefly generated in the fiber

core, where most of the pump power is absorbed. This can be obtained by calculating all the input and output optical powers flowing into and out of a unit volume at (r, z). Furthermore, $h(z)$ shows the convective coefficient, g ascertains the acceleration of gravity as well as N_u, G_r, and P_r which denote the Nusselt, Grashof, and Prandtl numbers, respectively. Moreover, d_c, μ_c, and κ_c accordingly depict the density, viscosity, and thermal conductivity of the coolant. Thus, the analytical expression for the Nusselt number is expressed below [40]:

$$N_u(z) = \left\{ 0.60 + \frac{0.387 \left[G_r(z) P_r \right]^{1/6}}{\left[1 + \left(0.559 / P_r \right)^{9/16} \right]^{8/27}} \right\}^2 \tag{31}$$

Since the highest temperature occurs at the fiber axis, it needs to pay more attention to the temperature behavior along the fiber axis. We then introduce T_{ave} as the longitudinally averaged temperature along the fiber axis, namely [27]:

$$T_{ave} = \frac{1}{L} \int_0^L T(r = 0, z) dz \tag{32}$$

At last, the dissipated heat across the whole fiber cross section is realized by [20]:

$$Q(z) = 2\pi \int_0^c q(r, z) r \, dr \tag{33}$$

Therefore, the heat converted from the optical power per unit length of fiber can be compared under different pumps and fiber conditions. Herein, there is no any analytical solution and Eqs (24)–(26) can be solved numerically using the finite element method (FEM).

In 2004, Wang et al. [10] showed that lower operating temperature and more uniform heat dissipation in fibers can be obtained by optimizing the arrangement of pump powers, pump absorption coefficients, and fiber lengths through the distributed side–pumping mode. As a beneficial solution for a traditional end–pumped scheme, the arrangement of uneven pump absorption coefficients along the cavity can improve laser efficiency and reduce fiber temperature.

Figures 3 and 4 show the calculated temperature evolution in a typical Yb–doped double–clad fiber at the fiber axis ($r = 0$) and at the inner/outer cladding boundary ($r = 125$ μm) with uniform as well as non–uniform pump absorption coefficients. From these figures, one can reach the conclusion that the temperature difference in the radial direction is much smaller than in the axial direction. However, the average temperature is very high at the fiber end faces.
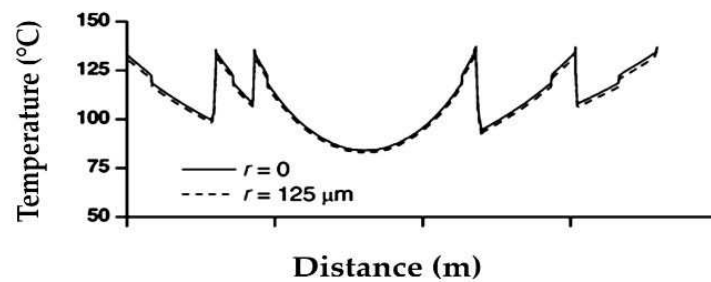
Figure 3. Temperature distribution in a 32–m fiber under an end–pump scheme with non–uniform pump absorption coefficients in five segments [10].
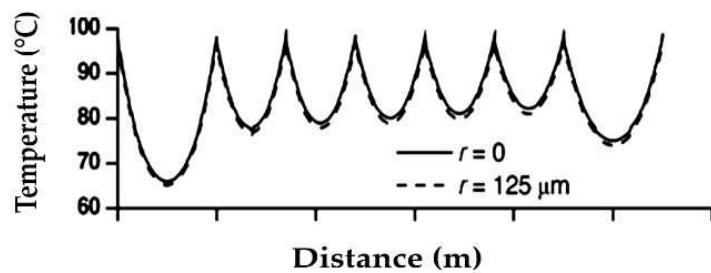

Figure 4. Temperature distribution in a 55–m fiber under a distributed side–pumped scheme with a uniform pump absorption coefficient of 1.2 dB/m, in seven segments [10].

In addition, the uneven temperature distribution results from non–uniform pump absorption in the fiber.

2.1.3. Radiative heat transfer

When the temperature of a body rises, three dominant thermal effects can be seen in it: convection, conduction, and the radiation. The latter process is in the form of electromagnetic radiation emitted by a heated surface in all directions. It travels directly to its point of absorption at the speed of light [35]. The total radiant heat energy radiated by a surface at a temperature greater than absolute zero is proportional to the Stefan–Boltzmann law. Usually, at high pump powers, the process of heat transfer is not only dominated by convection, but also being employed with radiation. The radiative heat transfer has to be considered in the thermal, stress, and thermo–optic analyses of any type of high–powered fiber lasers.

The procedure of heat dissipation from the fiber core to the fiber periphery is illustrated in Figure 5. At first, the heat generated in the fiber core is transferred to the surface by thermal conduction, and then dissipated to the ambient air by convective and radiative heat transfer. There are no heat sources in both the fiber inner and outer claddings.

For isotropic medium, the heat transfer between the surface of the fiber and the surrounging medium is given by [41]:

$$Q_c = 2\pi c L h_c \left(T \big|_{r=c} - T_\infty \right) \tag{34}$$

where the convective heat transfer coefficient (h_c), can be obtained from the following equation:
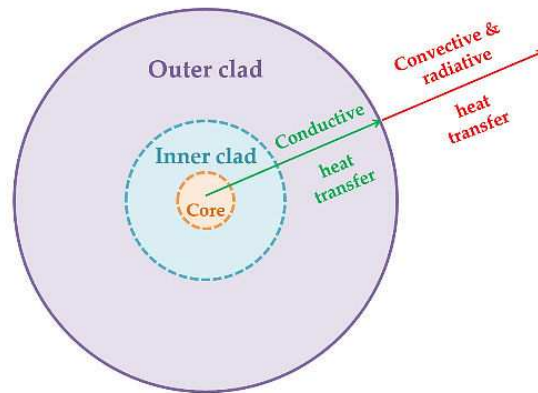
$$h_c = 0.5 N_u \kappa c \tag{35}$$

Figure 5. Model of heat dissipation in a double–clad fiber.

Also, the radiative heat transfer can be calculated using:

$$Q_r = 2\pi c L \varepsilon \sigma_b \left(T \big|_{r=c}^4 - T_\infty^4 \right) \tag{36}$$

where L is the fiber length, $T \big|_{r=c}$ ascertains the temperature at the surface of the fiber, T_∞ the environmental temperature, ε the surface emissivity, and σ_b denotes the Stefan–Boltzmann constant of the fiber material.

For a more convenient course of calculation, the radiative heat transfer coefficient (h_r) can also be described as:

$$Q_r = 2\pi c L h_r \left(T \big|_{r=c} - T_\infty \right) \tag{37}$$

In other words, the value of (h_r) can be clarified from:

$$h_r = \frac{\varepsilon \sigma_b \left(T \big|_{r=c}^4 - T_\infty^4 \right)}{T \big|_{r=c} - T_\infty} \tag{38}$$

Eventually, the total heat transfer is a summation of the convection and radiation heat transfers as follows:

$$Q = Q_c + Q_r = 2\pi cLh\left(T\big|_{r=c} - T_\infty\right) \tag{39}$$

where

$$h = h_c + h_r \tag{40}$$

It can see from Figure 6 that radiative heat transfer strictly increases with temperature, while convection remains almost constant during pumping. For this reason, the total heat transfer coefficient is affected more by radiation [40]. From the data in the curve, the h_c coefficient possesses non–linear variation when the temperature difference between the surface of the fiber and the environment is below 100 °C. This means that the effect of convection heat transfer is dominant at low temperature domains.
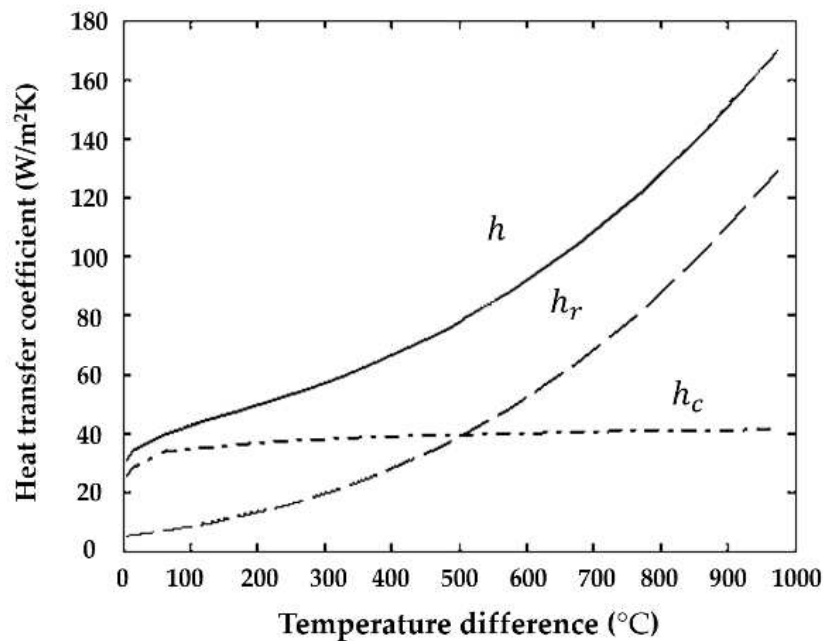

Figure 6. Heat transfer coefficients h_c, h_r, and h as the temperature difference between the surface of the fiber and the environment varies from 5 to 975 °C [40].

2.2. Pulsed regime

Contrary to CW mode, the analytical expressions for the temperature portion in individual fiber regions for the pulsed operating system are given by:

$$\rho c_v \frac{\partial T_1(r,\varphi,z,t)}{\partial t} - \kappa_1 \nabla^2 T_1(r,\varphi,z,t) = \eta P_v(r) \qquad 0 \le r \le a \tag{41}$$

$$\rho c_v \frac{\partial T_2(r,\varphi,z,t)}{\partial t} - \kappa_2 \nabla^2 T_2(r,\varphi,z,t) = 0 \qquad a \le r \le b \tag{42}$$

$$\rho c_v \frac{\partial T_3(r,\varphi,z,t)}{\partial t} - \kappa_3 \nabla^2 T_3(r,\varphi,z,t) = 0 \qquad b \le r \le c \tag{43}$$

where η represents the quantum efficiency and the average pump power absorbed per unit volume is demonstrated by $P_v(r)$. Here, the heat produced by multiple pulses or pump, simulates utilizing the time–dependent convection heat transfer equation in the dynamic regime.

At the first approximation, we assume that the absorbing region of the fiber is long enough and the rate of change of the absorption product is small enough, so that the longitudinal temperature gradient within the doped region is small. The ratio of the rate of heat flows out of the ends of the doped zone to that of the sides of the doped region after an instantaneous heating process effectively scales as the ratio of the dopant radius to the length of gain fiber. Consequently, at a given location z along the fiber, heat flows mostly radially, and at all times, $t > 0$, the z–dependence of $T(r, \varphi, z, t)$ is the same as that of the initial temperature profile $T(r, \varphi, z)$. In the following, we therefore omit the z–dependence in our notation for the sake of simplicity. As the fiber cools down, by supposing the azimuthal symmetry, the spatial and temporal evolution of the core temperature distribution is described by the homogeneous heat conduction equation [42] with a source term:

$$\rho c_v \frac{\partial T(r,t)}{\partial t} - \kappa \nabla^2 T(r,t) = \eta P_v(r) \tag{44}$$

The general solution is proposed in the following form [16]:

$$\Delta T(r,t) = \sum_{m=1}^{\infty} a_m(t) J_0\left(\frac{p_m r}{b}\right) exp\left(\frac{-t}{\tau_m}\right) \tag{45}$$

where $\Delta T(r, t) = T(r, t) - T_0$ explains the temperature rise profile, T_0 denotes the equilibrium temperature of the surrounding medium, and the time constants τ_m namely:

$$\tau_m = \frac{\rho c_v}{\kappa} \frac{b^2}{p_m^2} \tag{46}$$

The coefficients $a_m(t)$ and p_m are determined by two boundary conditions. The first one is energy conservation; presuming that cooling is due to natural air convection and, the heat flowing out of the fiber (at $r = b$) is proportional to the temperature difference between the fiber and the periphery air. The proportionality factor is the heat transfer coefficient h. This condition can be expressed as:

$$-\kappa \nabla T(r,t)\big|_{r=b} = h\big[T(r=b,t) - T_0\big] \tag{47}$$

Substituting the general solution Eq. (45) into Eq. (47) yields:

$$p_m J_1(p_m) = \frac{hb}{\kappa} J_0(p_m) \tag{48}$$

which determines the values of p_m.

The second boundary condition is at $t = 0$; supposing the temperature distribution at any time equals that of the initial time. Multiplying both sides of Eq. (45) by $r J_0(p_n r / b)$ and integrating in r across the fiber while applying Eq. (48) yields the time–dependent amplitudes $a_m(t)$ which are the solutions of:

$$\frac{\partial a_m}{\partial t} = \frac{\int_0^b \dfrac{P_\upsilon(r)}{\rho c^\upsilon} J_0\left(\dfrac{p_m r}{b}\right) r\, dr}{\dfrac{b^2}{2} J_0^2(p_m)\left[1 + \left(\dfrac{bh}{\kappa p_m}\right)^2\right]} \exp\left(\frac{t}{\tau_m}\right) \tag{49}$$

with $a_m(t=0)=0$.

In the particular case of a step pump profile of radius s [$P_\upsilon(r) = P_\upsilon$ for $r < s$ and 0 for $r > s$], this explanation becomes:

$$\Delta T(r,t) = \frac{2sb\eta P_\upsilon}{\kappa} \sum_{m=1}^{\infty} \frac{J_1\left(\dfrac{p_m s}{b}\right)}{p_m^3 J_0^2(p_m)} \frac{1 - \exp\left(\dfrac{-t}{\tau_m}\right)}{1 + \left(\dfrac{bh}{\kappa p_m}\right)^2} J_0\left(\frac{p_m r}{b}\right) \tag{50}$$

Assuming $\eta = 1$, the radial temporal evolution of the temperature profile at different times is shown in Figure 7. Shortly after the pump is turned on, the heat and the temperature increment are mostly confined to the vicinity of the core. As time goes on, the temperature at the center

of the fiber grows, and as heat flows outward, the temperature rise spreads toward the fiber edge. Eventually, the temperature profile becomes nearly uniform.
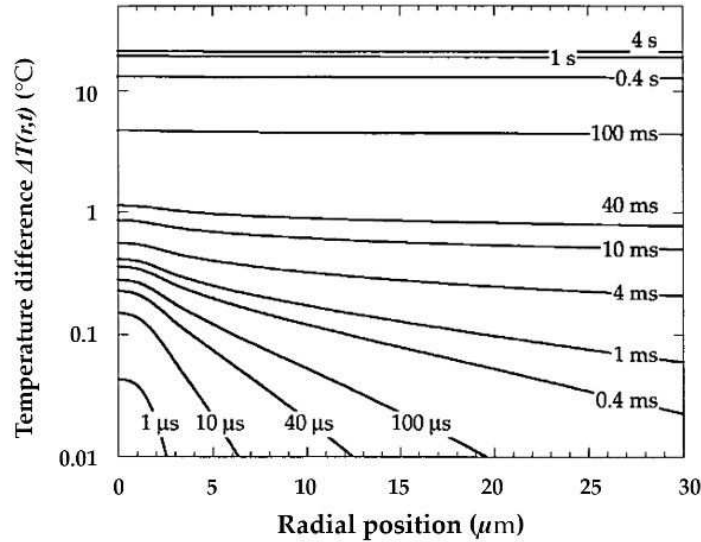

Figure 7. Radial temperature profile in a fiber at various times, $t > 0$, assuming that at time $t = 0$, the fiber begins to absorb 10 mW/cm of power in a doped region of 2 μm radius [16].

In the cladding regions, a_m is a time–independent coefficient which is determined as follows:

$$a_m = \frac{2}{b^2 J_0^2(p_m)\left(1 + (bh/\kappa p_m)^2\right)} \int_0^b \Delta T(r,0) J_0\left(\frac{p_m r}{b}\right) r\, dr \tag{51}$$

3. Cooling mechanisms

Fiber lasers and amplifiers have proven themselves as reliable systems with excellent beam quality and high output power. From the numerical and analytical analyses, one can conclude that the thermal effects must be considered at high–power regimes. Therefore, effective heat dissipation is a significant factor, with the aim of preventing damage to the fiber ends, interfaces, and coating. In order to suppress thermal issues, a suitable cooling method can be considered. This section remarks on the fast chilling of optical components and splices in order to modify their practical design, therefore, obtaining an optimum situation.

Heat generated in high–power fiber laser amplifiers is the source of increased temperature and stress inside the gain medium, which causes poor beam quality and restricts average output power. To solve this problem, fiber structures with enhanced mode areas have been suggested. These novel high–power schemes rely on multimode fibers with large diameter cores [43–44] or the amplification process takes place in a fiber cladding [45]. However, even if a high–quality beam is required, they are ultimately restricted by thermal effects.

Furthermore, a significant limiting factor in fiber laser amplifiers under strong pumping conditions is the temperature increase, growing the unsaturable loss mechanism. Effective heat extraction can reduce the temperature–dependent unsaturable losses especially in bismuth–doped fibers, resulting in increased laser performance [46]. In the case of rare–earth ions, unsaturable absorption losses can produce quenching processes such as cross–relaxation and up–conversion [47]. This can lead to wasting of the pump energy, raising the laser threshold, as well as reducing the conversion efficiency.

It is worth mentioning that cryogenically cooled systems promise a revolution in power scalability while maintaining good beam quality because of significant improvements in efficiency and thermo–optic properties. This is particularly true for Yb lasers due to their relatively low quantum defect as well as their broadband absorption spectrum even at cryogenic temperatures [48]. Amplification in Yb–doped fibers is generally possible from 976 nm to 1200 nm, but below 1030 nm it becomes more challenging, since the absorption cross section grows towards shorter wavelengths [49]. This thermal population and thus absorption in the wavelength range above 1000 nm can be significantly alleviated by cooling the fiber to low temperatures [50].

In addition to this, any surface cooling creates a thermal gradient that strains the laser medium as well as distorts optical waves. Lowering of the doping concentration and increasing of the fiber length make the cooling easier, but enhance non–linear effects such as SBS and SRS, which can deplete the amplified signal. An appropriate way to overcome this challenge is by using the anti–Stokes cooling method for spontaneous and stimulated emission radiation–balanced lasers, mentioned by Steven R. Bowman in 1999 [51–52]. Hereupon, the thermal load generated from stimulated emission can be dissipated thoroughly, which permits lasing without detrimental heating of the laser medium.

From another point of view, lower operating temperatures and more uniform heat dissipation at ambient temperature can be achieved by optimizing the arrangement of pump powers, pump absorption coefficients, and fiber lengths [10], presuming a distributed side–pumping mode in passive cooling systems. Additionally, forced chilling methods comprising passive air cooling [53] and active liquid cooling [54–55] through convectional processes, as well as conductive thermoelectric (Peltier) effects [56] using cold plates or heat sinks are noticeable techniques, and thereby a number of detrimental thermal effects can be effectively suppressed.

The liquid chilled thermal management is commonly performed by means of cold water, fluorocarbon refrigerants, ethylene glycol, commercial silicone fluids, and any electronic coolants or the like [54]. Although water cooling has proved to be very efficient at dissipating heat and is extensively adopted for most high–power, solid–state lasers, it cannot be directly applied to most Yb–doped double–clad arrays. For fibers with limited chemical stability such as, fluoride fibers, water cooling should be avoided. However, air cooling is a good candidate for many applications due to its compact structure and moderate dissipating efficiency [20].

In general, for efficiently cooling a system, the exothermic components which have any significant heat load, including high–power laser diodes, integrated combiners, splice points, optical reflectors, as well as doped fibers can be immersed or placed in contact with a thermal

sink of appropriate temperature [57]. In 2011, Fan et al. [13] introduced a copper heat sink with various geometries in order to chill a doped fiber, something which was critical for the reliability of their high–power operation. The thermal contact resistance per unit surface $R_{tc}''(m^2 K/W)$ between the fiber and the heat sink is expressed as [58]:

$$R_{tc}'' = \frac{T_s - T_\infty}{q''} \tag{52}$$

where $T_s(K)$ is the fiber surface temperature, $T_\infty(K)$ the heat sink temperature, and $q''(W/m^2)$ the heat flux. In fact, Eq. (52) suggests the concept for the treatment of the heat flow through a fiber layer by analogy to the diffusion of electrical charge [12], where the temperature difference is analogous to the electrical voltage which drives the heat flow through a thermal resistant. For an active fiber, the heat generation, $q_0(W/m^3)$, the heat load $q'(W/m)$, and the pump absorption $\alpha(dB/m)$ are related to each other [59]:

$$q_0 = \left(1 - 10^{-\alpha \cdot \frac{dL}{10}}\right) = \frac{P\left(1 - \lambda_p/\lambda_s\right)}{\pi a^2} = \frac{q' dL}{\pi a^2} \tag{53}$$

where P represents the pump power through a section of length dL, and λ_s and λ_p display the signal and pump wavelengths, respectively. Moreover, q'' is defined by $q'/perimeter$.

However, at moderate temperatures higher than ~-30 °C, a novel dry–ice chiller [60–61] is preferred. The practical scheme of a dry–ice heat exchanger being used as fast–cooling equipment for hot optical components is based on the cryogenic powder mixture using ethylene glycol to supply a high–capacity chilling bath, attaining thermal equilibrium for a long while. At the beginning of this process, the dry–ice/glycol bath creates a boiling gel to reduce the temperature to a few degrees as long as the dry–ice debris is available in the coolant. When thermal exchange between dry–ice and glycol takes place, the boiling goes on and the gel temperature drops from -30 °C to ~300 K [62], depending on the dry–ice loading.

Otherwise, while scaling up the power in high–power or high–energy domains, cryogenic lasers [63] may be required where in general terms, the gain medium is operated at cryogenic temperatures through liquefied gases including ammonia (~240 K), liquid CO_2 (~195 K), methane (~111 K), liquid nitrogen (~77 K), liquid neon (~27 K), or even liquid helium (~4 K).

The spectral properties of the amorphous glass host material are strongly affected by temperature [50] and one can illustrate how cryogenic cooling methods are employed to dramatically raise the efficiency and the stability of fiber laser amplifiers [64] as well as to efficiently diminish self–pulsing at the price of a spectrally broad emission spectrum. The justification is that the gain cross section of dopant ions becomes greater for various inversions under cryogenic chilling by means of optical refrigeration. In addition, this is believed to be related to the reduction of the thermal population in the upper stark levels of manifold, so that reabsorption at the signal wavelength completely eradicates. This enables the use of a considerably longer fiber length, which could entirely absorb the pump light.

Besides this, spectral density decreases as linewidth increases. The rising in linewidth is believed to be a result of the alleviating the homogeneous broadening due to the lowered operating temperature. To prevent this detrimental problem and achieve a temporally stable, narrow linewidth, highly efficient laser, a volume Bragg grating [23] can be used according to Figure 8. By efficiently cooling an active gain media, the thermal population and therefore the reabsorption losses drop, shifting the preferred lasing beam toward shorter wavelengths [11]. For cryogenically cooling fiber sources, the gain material can easily be submerged in the coolant.
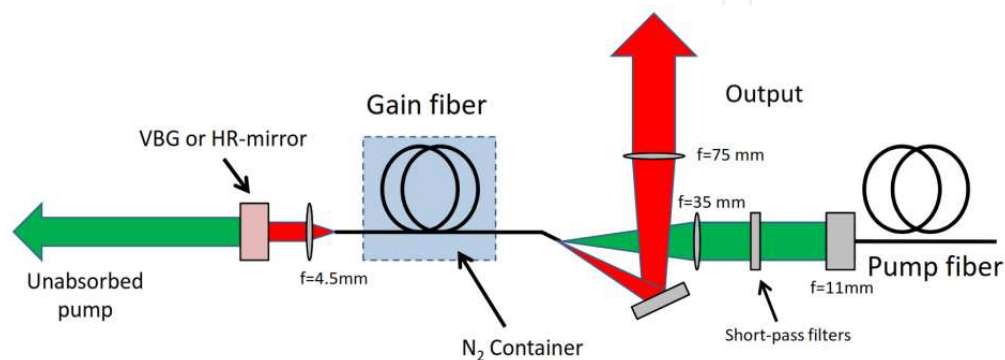
Figure 8. Cryogenically cooled fiber laser [64].

In 2006, Seifert et al. intensely reduced the thermal population of the lower laser levels of a Yb–doped fiber amplifier by using cryogenic cooling [65]. One year later, the temperature effect on the emission properties of Yb–doped optical fibers was investigated by Newell et al. They revealed that chilling efficiently eradicates the absorption tail above 1 μm [50]. Moreover, cooling of gain media using liquefied gases drastically limits the destructive third–order non–linear self–pulsing [22] effect. These results show that cryogenic cooling of Yb–doped fiber lasers is a simple way to stabilize the temporal output as well as substantially enhance the efficiency.

Author details

Maryam Eilchi[1*] and Parviz Parvin[2]

*Address all correspondence to: m_ilchi@aut.ac.ir

1 Laser and Optics Research Institute, Nuclear Science and Technology Research Institute, Tehran, Iran

2 Photonic Engineering Group, Department of Physics, Amirkabir University of Technology, Tehran, Iran

References

[1]   S. Yin, P. Yan, and M. Gong. End-pumped 300 W continuous-wave ytterbium-doped all-fiber laser with master oscillator multi-stage power amplifiers configuration. *Opt. Express.*2008; 16(2): 17864–17869.

[2]   J. Richardson, J. Nilsson, and W. A. Clarkson. High-power fiber lasers: Current status and future perspectives. *J. Opt. Soc. Am. B*. 2010; 27(11): B63–B92.

[3]   Y. Jeong, J. Sahu, D. Payne, and J. Nilsson. Ytterbium-doped large-core fiber laser with 1.36 kW continuous wave Output power. *Opt. Express*. 2004; 12(25): 6088–6092.

[4]   E. Stiles. New developments in IPG fiber laser technology. In: 5th International Workshop on Fiber Lasers: 2009.

[5]   B. He, J. Zhou, Q. Lou, Y. Xue, Z. Li, W. Wang, J. Dong, Y. Wei, and W. Chen. 1.75 killowatt continuous wave output fiber laser using homemade ytterbium-doped large-core fiber. *Microw. Opt. Technol. Lett.*2010; 52(7): 1668–1671.

[6]   C. Wirth, O. Schmidt, I. Tsybin, et al. 2 kW incoherent beam combining of four narrow-linewidth photonic crystal fiber amplifiers. *Opt. Express*. 2009; 17(3): 1178–1183.

[7]   Available from: *http://www.IPGPhotonics.com*

[8]   M. Ilchi-Ghazaani and P. Parvin. Distributed scheme versus MOFPA array on the power scaling of a monolithic fiber laser. *IEEE J. Quant. Electron*. 2014; 50(8): 698–708.

[9]   D. C. Brown and H. J. Hoffman. Thermal, stress, and thermal-optic effects in high average power double-clad silica fiber lasers. *IEEE J. Sel. Top. Quantum Electron*. 2001; 37(2): 207–217.

[10] Y. Wang, C. Q. Xu, and H. Po. Thermal effects in kilowatt fiber lasers. *IEEE Photon. Technol. Lett.*2004; 16(1): 63–65.

[11] N. A. Brilliant and K. Lagonik. Thermal effects in a dual-clad ytterbium fiber laser. *Opt. Lett.*2001; 26(21): 1669–1671.

[12] M. A. Lapointe, S. Chatigny, M. Piché, M. Cain-Skaff, and J. N. Maran. Thermal effects in high power CW fiber lasers. In: *Proc. SPIE. 719511U*: 2009. DOI: 10.1117/12.809021.

[13] Y. Fan, B. He, J. Zhou, J. Zheng, H. Liu, Y. Wei, J. Dong, and Q. Lou. Thermal effects in kilowatt all-fiber MOPA. *Opt. Express*. 2011; 19(16): 15162–15172.

[14] Y Huo and P. Cheo. Thermomechanical properties of high-power and high-energy Yb-doped silica fiber lasers. *IEEE Photon. Technol. Lett*. 2004; 16(3): 759–761.

[15] L. Zenteno. High-power double-clad fiber lasers. *J. Lightwave Technol*. 1993; 11: 1435–1446.

[16] M. K. Davis, M. J. F. Digonnet, and R. H. Pantell. Thermal effects in doped fibers. *J. Lightwave Technol.*1998; 16: 1013–1023.

[17] Rumao Tao, Pengfei Ma, Xiaolin Wang, Pu Zhou and Zejin Liu. 1.3 kW monolithic linearly polarized single-mode master oscillator power amplifier and strategies for mitigating mode instabilities. *Photon. Res.* 2015; 3(3): 86–93.

[18] B. Ward, C. Robin, and I. Dajani. Origin of thermal modal instabilities in large mode area fiber amplifiers. *Opt. Express.* 2012; 20: 11407–11422.

[19] W. W. Ke, X. J. Wang, X. F. Bao, and X. J. Shu. Thermally induced mode distortion and its limit to power scaling of fiber lasers. *Opt. Express.* 2013; 21: 14272–14281.

[20] Y. Wang. Heat dissipation in Kilowatt fiber power amplifiers. *IEEE J. Quantum Electron.*2004; 40(6): 731–740.

[21] V. Ashoori and A. Malakzadeh. Explicit exact three-dimensional analytical temperature distribution in passively and actively cooled high-power fibre lasers. *J. Phys. D. Appl. Phys*. 2011; 44(35): 1–6.

[22] K. Sumimura, H. Yoshida, H. Okada, H. Fujita, and M. Nakatsuka. 2007. Suppression of self-pulsing in Yb-doped fiber lasers with cooling by liquid nitrogen. In: Lasers and Electro-Optics – Pacific Rim; 2007; CLEO/Pacific Rim. pp. 1–2.

[23] P. Jelger, K. Seger, V. Pasiskevicius, and F. Laurell. Highly efficient temporally stable narrow linewidth cryogenically cooled Yb-fiber laser. *Optics express*. 2009; 17(10): 8433–8438.

[24] M. El H. Assad and D. C. Brown. Thermodynamic analysis of end-pumped fiber lasers subjected to surface cooling. *IEEE Journal of Quantum Electronics*. 2013; 49(1): 100–107.

[25] D. C. Hanna, M. J. McCarthy, and P. J. Suni. Thermal considerations in longitudinally pumped fibre and miniature bulk lasers. In: *Boston. Proc. Fiber Laser Sources and Amplifiers: SPIE 1171*; 1990. pp. 160–166. DOI: 10.1117/12.963149

[26] D. C. Brown and H. J. Hoffman. Thermal, stress, and thermo-optic effects in high average power double-clad silica fiber lasers. *IEEE J. Of Quantum Electron*. 2001; 37(2): 207–217.

[27] Y. Wang, C. Q. Xu, and H. Po. Analysis of Raman and thermal effects in kilowatt fiber lasers. *Opt. Commun*. 2004; 242(4): 487–502.

[28] P. Elahi and N. Zare. The analytical solution of rate equations in end-pumped fiber lasers with minimum approximation and temperature distribution during the laser operation. *Acta Phys. Pol. A*. 2009; 116(4): 522–524.

[29] Y. Huang, H. Tsai, and F. Chang. Thermo-optic effects affecting the high pump power end pumped solid state lasers: Modeling and analysis. *Opt. Commun*. 2007; 273: 515–525.

[30] M. Sabaeian, H. Nadgaran, M. De Sario, L. Mescia, and F. Prudenzano. Thermal effects on double clad octagonal Yb:glass fiber laser. *Opt. Mater*. 2009; 31: 1300–1305.

[31] P. Li, C. Zhu, S. Zou, H. Zhao, D. Jiang, G. Li, and M. Chen. Theoretical and experimental investigation of thermal effects in a high power Yb^{3+}-doped double-clad fiber laser. *Opt. Laser Technol*. 2008; 40: 360–364.

[32] Z. Mohammed, H. Saghafifar, and M. Soltanolkotabi. An approximate analytical model for temperature and power distribution in high-power Yb-doped double-clad fiber lasers. *Laser Phys*. 2014; 24: 115107–115119.

[33] Z. Mohammed and H. Saghafifar. Optimization of strongly pumped Yb-doped double-clad fiber lasers using a wide-scope approximate analytical model. *Opt. Laser Technol*. 2014; 55: 50–57.

[34] D. Xue. Three-dimensional simulation of the temperature field in high-power double-clad fiber laser. *Optik*. 2011; 122: 932–935.

[35] J. Li, K. Duan, Y. Wang, X. Cao, W. Zhao, Y. Guo, and X. Lin. Theoretical analysis of the heat dissipation mechanism in Yb^{3+}-doped double-clad fiber lasers. *Journal of Modern Optics*.2008; 55(3): 459–471.

[36] P. Parvin, M. Ilchi-Ghazaani, A. R. Bananej, and Z. Lali-Dastjerdi. Small signal gain and saturation intensity of a Yb:Silica fiber MOPA system. *Journal of Optics & Laser Technology (JOLT)*.2009; 41: 885–891.

[37] M. Ilchi-Ghazaani and P. Parvin. Impact of cavity loss on the performance of a single-mode Yb:silica MOFPA array. *Optics & Laser Technology*. 2015; 65: 94–105.

[38] S. Mohammadian, P. Parvin, M. Ilchi-Ghazaani, R. Poozesh, and K. Hejaz. Measurement of gain and saturation parameters of a single-mode Yb:silica fiber amplifier. *Optical Fiber Technology*. 2013; 19: 446–455.

[39] M. Abouricha, A. Boulezhar, and N. Habiballah. The comparative study of the temperature distribution of fiber laser with different pump schemes. *Open Journal of Metal*.2013; 3: 64–71.

[40] P. Yan, A. Xu, and M. Gong. Numerical analysis of temperature distributions in Yb-doped double-clad fiber lasers with consideration of radiative heat transfer. *Opt. Eng.* 2006; 45(12): 124201 1–4.

[41] J. P. Holman. Heat Transfer (8th edition).McGraw-Hill, New York, 1997.

[42] C. Kittel and H. Kroemer. Thermal Physics (2nd edition). W. H. Freeman, New York, 1980, pp. 424–430.

[43] R. I. Epstein, M. I. Buchwald, B. C. Edwards, T. R. Gosnell, and C. E. Mungan. Observation of laser-induced fluorescent cooling of a solid. *Nature* (London). 1995; 377: 500–502.

[44] D. Taverner, D. J. Richardson, L. Dong, J. E. Caplen, K. Williams, and R. V. Penty. 158-µJ pulses from a single-transverse-mode, large-mode-area erbium-doped fiber amplifier. *Opt. Lett*. 1997; 22(6): 378–380.

[45] G. Nemova and R. Kashyap. High-power long period grating assisted EDFA. *J. Opt. Soc. Am. B*.2008; 25: 1322–1327.

[46] M. P. Kalita, S. Yoo, and J. K. Sahu. Influence of cooling on a bismuth-doped fiber laser and amplifier performance. *Applied Optics*.2009; 48(30): G83–G87.

[47] M. E. Davis, M. J. F. Digonnet, and R. H. Pantell. Characterization of clusters in rare earth-doped fibers by transmission measurements. *J. Lightwave Technol*. 1995; 13: 120–126.

[48] Y. Fan, D. J. Roshan, L. Aggarwal, J. R. Ochoa, B. Chann, M. Tilleman, and J. Spitzberg. Cryogenic Yb^{3+}-doped solid-state lasers. *IEEE Journal of Selected Topics in Quantum Electronics*.2007; 13(3): 448–459.

[49] R. Paschotta, J. Nilsson, A. C. Topper, and D. C. Hanna. Ytterbium-doped fiber amplifiers. *IEEE J. Quantum Electron*. 1997; 33: 1049–1056.

[50] T. C. Newell, P. Peterson, A. Gavrielides, and M. P. Sharma. Temperature effects on the emission properties of Yb-doped optical fibers. *Opt. Commun*. 2007; 273: 256–259.

[51] S. R. Bowman. Laser without internal heat generation. *J. Lightwave Technol*. 1999; 35: 115–122.

[52] G. Nemova and R. Kashyap. Optimization of the dimensions of an Yb^{3+}:ZBLANP optical fiber sample for laser cooling of solids. *Optics Letters*.2008; 33(19): 2218–2220.

[53] S. Sakuragi, M. Saitoh, H. Kotani, and K. Imagawa. Cooling mechanism for optical fiber. US Patent. Patent Date: February 25, 1986; Patent No. US 4,572,609.

[54] J. A. Davis. Systems and methods of cooling a fiber amplifier with an emulsion of phase change material. US Patent. Patent Date: November 25, 2008; Patent No. US 7,457,502 B2.

[55] S. Tokita, M. Murakami, S. Shimizu, M. Hashida, and S. Sakabe. Liquid-cooled 24 W mid-infrared Er:ZBLAN fiber laser. *Opt. Lett*. 2009; 34(20): 3062–3064.

[56] L. Li, H. Li, T. Qiu, V. L. Temyanko, M. M. Morrell, A. Schülzgen, A. Mafi, J. V. Moloney, and N. Peyghambarian. 3-dimensional thermal analysis and active cooling of short-length high-power fiber lasers. *Opt. Express*. 2005; 13(9): 3420–3428.

[57] J. E. Rothenberg, S. J. Brosnan, and T. Epp. High efficiency, high power cryogenic laser system. Patent Application Publication. Publication Date: August 30, 2007;Pub. No. US 2007/0201518 A1.

[58] Y. Fan, S. Dai, B. He, C. Zhao, J. Zhou, Y. Wei, J. Zheng, and Q. Lou. Efficient heat transfer in high-power fiber lasers. *Chinese Optics Letters (COL)*.2012; 10(11): 111401 1–4.

[59] Lapointe, S. Chatigny, M. Piché, M. Cain-Skaff, J. Maran. Thermal effect in high power CW fiber lasers. In: *Proc. of SPIE*. 7195. 71951U-1; 2009. DOI: 10.1117/12.809021.

[60] P. Parvin and M. Ilchi-Ghazaani. Modified Dry Ice Heat Exchanger for Heat Removal of Portable Nuclear Reactors. Non Provisional US Patent. Filling Date: 05/14/2012 (Application No. US 13/470,547).

[61] M. Ilchi-Ghazaani and P. Parvin. Characterization of a dry ice heat exchanger. *International Journal of Refrigeration*. 2011; 34(3): 1085–1097.

[62] Do. W. Lee and C. M. Jensen. Dry-ice bath based on ethylene glycol mixtures. *Journal of Chemical Education*. 2000; 77(5): 629–629.

[63] R. Steinborn, A. Koglbauer, P. Bachor, T. Diehl, D. Kolbe, M. Stappel, and J. Walz. A Continuous wave 10 W cryogenic fiber amplifier at 1015 nm and frequency quadrupling to 254 nm. *Optics Express*.2013; 21(19): 22693–22698.

[64] P. Jelger. High Performance Fiber Lasers with Spectral, Thermal and Lifetime Control [thesis]. Stockholm, Sweden: Department of applied physics, KTH, Royal Institute of Technology,2009.

[65] A. Seifert, M. Sinther, T. Walther, and E. S. Fry. Narrow-linewidth, multi-Watt Yb-doped fiber amplifier at 1014.8 nm. *Appl. Opt*. 2006; 45: 7908–7911.